Physical and one-dimensional properties of single-crystalline La_5AgPb_3

Jannis Maiwald* and M. C. Aronson
Quantum Matter Institute, University of British Columbia, Vancouver, BC, Canada V6T 1Z4
and Department of Physics and Astronomy, University of British Columbia, Vancouver, BC, Canada V6T 1Z4

(Received 29 September 2021; revised 23 March 2022; accepted 28 March 2022; published 8 April 2022)

We report here the properties of single crystals of La_5AgPb_3, which is a member of the R_5MX_3 (R = rare earth, M = transition metal or main group element, X = Pb, Sn, Sb, In, Bi) family of chainlike compounds. Measurements of the electrical resistivity, specific heat, and magnetic susceptibility are compared to the results of density functional calculations, finding that La_5AgPb_3 is a nonmagnetic metal with moderate correlations. The analysis of the electrical resistivity and specific heat measurements highlight the importance of lattice vibrations in the material, while the calculated electron density suggests the presence of localized La and well-hybridized Ag orbitals that extend along the c axis in the La_5AgPb_3 structure. The temperature dependence of the magnetic susceptibility is consistent with a possible one-dimensional character of La_5AgPb_3, where the strength of correlations is much weaker than in one-dimensional conductors that have been previously reported.

DOI: 10.1103/PhysRevB.105.155116

I. INTRODUCTION

Rare-earth based intermetallic compounds feature significant electronic correlations, which lead to a host of fascinating ordered or disordered phases, such as complex, at times frustrated, magnetism, superconductivity, and quantum phase transitions [1–3]. Of particular interest are low-dimensional or geometrically frustrated materials, where quantum fluctuations can overwhelm the tendency to adopt ordered ground states. In these cases, the normal metallic behavior found in conventional conductors is replaced by ground states with unconventional excitations, such as fractionalized excitations. One-dimensional systems are of particular interest, due to the body of theoretical results that can be tested in real materials using inelastic neutron scattering [4,5], and angle resolved photoemission [6,7].

While most experimental work has been carried out so far on insulating spin chain systems, there is a pressing need to identify new materials where the physics of one dimension can be pursued in systems where electronic correlations are not strong enough to lead to localized electrons and insulating behavior. In three-dimensional materials, reducing the strength of correlations leads to a Mott transition or crossover where the localized electrons become itinerant, and the moments collapse with the onset of a metallic phase. Investigations into whether a corresponding scenario occurs in one-dimensional systems have been pursued largely in organic conductors [8], and there is great interest in finding new classes of compounds where the interplay of low dimensionality and moderate correlation strengths may lead to novel excitations and new quantum phases.

In seeking new correlated systems with quasi-one-dimensionality, it is desirable to find a family of isostructural compounds where materials trends can be related to functionality, and where control over differing degrees of correlations is possible. The ternary compounds R_5MX_3 (R = rare earth, M = transition metal or main group element, X = Pb, Sn, Sb, In, Bi) present a promising example of such a family, having the main structural motif of quasi-infinite linear chains composed of confacial triangular antiprisms [9]. These compounds form with a rich variety of magnetic and nonmagnetic atoms such as R = Ce, Pr, Tb, Dy, Ho, Tm and X = Mn, Fe, Co, Ni. Accordingly, existing experimental work has found exceptionally rich magnetic behavior, with evidence for both highly localized magnetic moments, as well as increasing hybridization and resulting Kondo compensation of those moments [9–11].

We focus here on La_5AgPb_3, which is a nonmagnetic member of this class of materials. Previously unstudied, we assess its potential as a benchmark system of one-dimensional chains of moderately correlated electrons, whose spin and angular momentum provide the only entities that might support magnetism. Electronic structure calculations support the proposal that La_5AgPb_3 may be one-dimensional, and as well suggest a variety of compositional variants where both transition metal and rare-earth magnetism can be introduced. La_5AgPb_3 demonstrates Fermi liquid behavior in its low-temperature specific heat, with modest enhancements of the densities of states relative to values found in density functional theory (DFT) calculations. The temperature dependence of the magnetic susceptibility has a broad maximum, similar to those found in quasi-one-dimensional metals.

II. METHODS

Single crystals of La_5AgPb_3 were synthesized using a self-flux method. Elemental La (99.9%), Ag (99.999%), and Pb (99.999%) in a ratio of 6:6:1 were placed in an alumina crucible set equipped with a strainer and a catch crucible,

*jannis.maiwald@ubc.ca

 ©2022 American Physical Society

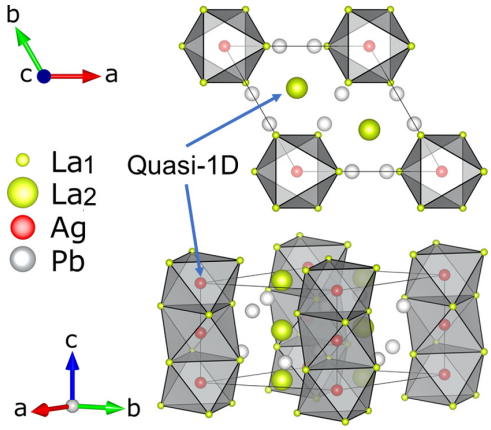

FIG. 1. The refined crystal structure of La_5AgPb_3. The unit cell (thin gray lines) is shown in (top) top view and (bottom) perspective view. La atoms on the La1 (6*g*) site were reduced in size for clarity. Arrows indicate quasi-one-dimensional arrangements of La2 and Ag, respectively.

which was then sealed under ∼300 mbar argon atmosphere in a quartz tube [12]. This assembly was subsequently heated at a rate of ∼330 °Ch^{-1} to 1030 °C where it remained for 3 h to ensure adequate mixing of the reactants. Single crystals were precipitated out of solution by lowering the temperature at a rate of 3°Ch^{-1} down to 930 °C. At that temperature, the tubes were removed from the furnace and were quickly placed upside down in a centrifuge, where the liquid flux was separated from the crystals by spinning at 2000 rpm for about 30s.

Using this procedure we were able to grow needlelike single crystals of La_5AgPb_3. Typical dimensions of the crystals are $4 \times 0.5 \times 0.5$ mm^3. The basal plane of the crystals is rectangular in shape with beveled edges. An image of the single crystal used for specific heat measurements is shown in the inset of Fig. 2.

We found La_5AgPb_3 to be air sensitive. The initially metallic luster of our single crystals turned to dull gray when exposed to air for a few minutes. Once the surface transformed there was no further change to the crystals, even after several days. However, an additional x-ray powder diffraction pattern taken on a powdered sample that had been exposed to air for about 2 weeks showed that La_5AgPb_3 fully breaks down, as the pattern can no longer be indexed with the reported structure. The new pattern (not shown) indicates that the main products of this breakdown are lanthanum hydroxide [$La(OH)_3$], lanthanum lead ($LaPb_3$), and lead(II) oxide (PbO). As a precaution sample preparations and measurements were carried out under protective argon or helium atmosphere (argon glovebox, airtight sample holder for x-ray diffraction, etc.). In case of resistivity, specific heat and magnetization measurement samples were only very briefly (<30 s) exposed to air as they were loaded into the respective measurement instrumentation.

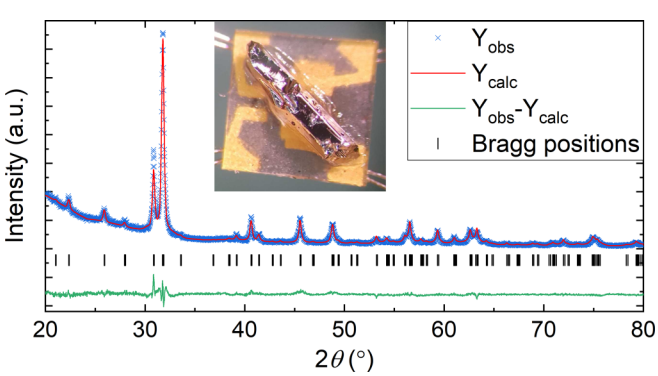

FIG. 2. Measured powder XRD pattern of as-grown La_5AgPb_3, and its refinement using the reported hexagonal structure with space group $P6_3/mcm$. Bragg peak positions are indicated. Note the background increase below 35° is due to the airtight sample holder. Inset: Optical microscope image of a La_5AgPb_3 single crystal (length ∼4 mm) mounted on a heat capacity platform.

Powder x-ray diffraction (XRD) patterns were recorded with a Bruker D8 Advance diffractometer in the Bragg-Bretano configuration using a Cu $K\alpha$ cathode with a Johansson monochromator that blocks any $K\alpha_2$ radiation. The powder diffraction patterns were refined with the FULLPROF software suite. Energy-dispersive x-ray (EDX) spectroscopy was performed on a Philips XL-30 scanning electron microscope equipped with at Bruker xFlash 10-mm^2 silicon drift detector. Measurements of the electrical resistivity and specific heat were carried out using a Physical Property Measurements System from Quantum Design equipped with a He^3/He^4 dilution refrigerator insert. Measurements of the magnetic susceptibility were performed using a Magnetic Property Measurements System 3 also from Quantum Design.

Band structure calculations were performed using the linear augmented plane wave code WIEN2K [13] (version 21.1) on the reported crystal structure with space group $P6_3/mcm$. The gradient-corrected density functional of Ref. [14] (Perdew-Burke-Ernzerhof) was used in all calculations. The self-consistent field cycles were computed using an optimized basis set size and k mesh of $R_{MT}k_{max} = 9$ and 5000 k points, respectively.

III. STRUCTURAL AND PHYSICAL PROPERTIES

A. Sample characterization

The ternary compounds R_5MX_3 (R = rare earth, M = transition metal or main group element, X = Pb, Sn, Sb, In, Bi) form in a hexagonal crystal structure with space group $P6_3/mcm$ (193) (Fig. 1) [15–17]. These systems feature quasi-one-dimensional arrangements of their constituent M atoms on the 2*b* sites and R atoms on the 4*d* sites that extend along the crystallographic *c* axis. The R atoms on the 6*g* site shield the M atoms from the X atoms by forming irregular octahedra (confacial trigonal antiprisms) around the X atoms. These materials form in the hexagonal Hf_5CuSn_3 structure, more broadly known as the Ga_4Ti_5 structure type, which is distinguished from the more populous Mn_5Si_3 structure type by the occupancy of the M site [9–11].

La_5AgPb_3 forms in the Hf_5CuSn_3 structure type, as depicted in Fig. 1. Layers of La (4*d* site, La2) and Pb are separated by layers of La (6*g* site, La1) and Ag that are stacked along the crystallographic *c* axis. The Hf_5CuSn_3 structure type is differentiated from the Mn_5Si_3 structure by the

TABLE I. Results—EDX analysis and Rietveld refinement with reduced $\chi^2_{red} = 3.42$ and R factors: $R_{wp}/R_{exp} = 8.3/4.5$. Note: Stated EDX uncertainties reflect the statistical error over several measurements and do not account for the systematic error of the scanning electron microscopy EDX technique.

Composition (at. %)	La	Ag	Pb
EDX average	57.8(3)	10.0(1)	32.2(4)
Nominal	55.6	11.1	33.3
Lattice parameters	a (Å)	c (Å)	V (Å^3)
La_5AgPb_3	9.7741(7)	6.8902(6)	570.06
Ref. [9]	9.560(1)	7.037(2)	556.97
Atomic coordinates	x	y	z
La1 (6g)	0.2739(4)	0	1/4
La2 (4d)	1/3	2/3	0
Ag (2b)	0	0	0
Pb (6g)	0.6220(3)	0	1/4

presence of the Ag atoms occupying the corners of the unit cell, vacant in the Mn_5Si_3 structure.

The Ag atoms on the 2b sites, as well as the La atoms on the 4d sites form linear chains. The La atoms on the La1 site form irregular octahedra around the Ag atoms on the 2b sites, effectively shielding them from the Pb atoms. This arrangement suggests that Ag-Pb bonding is weak, as expected considering the limited solid solubility of Ag and Pb. This type of behavior can frequently be observed when introducing a third element to an "antagonistic pair" of elements [18]. More importantly this structure in La_5AgPb_3 contributes to the formation of quasi-one-dimensional arrangements of the Ag and La2 sites along the crystallographic c axis (Fig. 1). Replacing the respective elements with magnetic elements in the future could provide a great opportunity to determine whether one-dimensional magnetism can be induced in this class of materials.

The composition of as-grown single crystals of La_5AgPb_3 was confirmed using EDX analysis. The mean composition, averaged over 19 measurement points, is given in Table I. The data all agree with the nominal composition of La_5AgPb_3, given a typical EDX resolution of a few percent.

The crystal structure of the synthesized La_5AgPb_3 crystals was verified by means of x-ray powder diffraction. The diffraction pattern of powdered single crystals of La_5AgPb_3 and its Rietveld refinement are compared in Fig. 2. All recorded diffraction peaks can be indexed within the hexagonal structure reported for polycrystals of La_5AgPb_3 [9,10]. The absence of extrinsic diffraction peaks rules out the presence of crystalline impurity phases with concentrations larger than $\simeq 1$ %. The largest differences between the refined structure and the powder XRD data are found near the strongest peak of La_5AgPb_3 near 30.8°, and are ascribed to preferential orientation of the crystallites in our powder. The refined lattice parameters and atomic coordinates are presented in Table I. The former show about a ± 2 % deviation from reported literature values. We attribute this difference to differences in sample preparation. The samples in Ref. [9] were prepared at significantly higher temperatures and over a much longer time, i.e., 13 days vs 3 days. Extended time at high temperature can have an effective tempering effect on the samples, which can lead to a positive or negative change in sample quality (defects, disorder, etc.). Our XRD measurements indicate that we have successfully grown stoichiometric high-quality single crystals of La_5AgPb_3.

B. Density functional calculations of the electronic structure

We have performed *ab initio* band structure calculations based on the local-spin-density approximation (LSDA) using the experimentally determined hexagonal crystal structure of La_5AgPb_3. We have included spin-orbit coupling (SOC) for all elements. DFT calculations tend to overestimate the hybridization of 4f states due to underestimated Coulomb repulsion of the localized 4f orbitals. Therefore, the energy of the unoccupied 4f states is too low and shifted too close to the Fermi energy. The unoccupied La 4f peak is experimentally centered around 5.5 eV [19,20], which is about 2.5 eV higher than in our bare LDA calculations. To correct for this we include an on-site Coulomb interaction (U) for La, to minimize the influence of the unoccupied La 4f states on the density of states (DOS) at the Fermi energy E_F. The Coulomb and exchange parameters were set to $U = 7.5$ eV and $J = 0$, respectively, leading to a 4f peak around 5.5 eV in our LSDA+U+SOC calculations (not shown). Note, this common correction is necessary in order to isolate any correlations that may arise from other sources. The calculated DOS and band structure of La_5AgPb_3 are depicted in Fig. 3.

These calculations indicate that La_5AgPb_3 is a metal, with five bands crossing the Fermi level [Fig. 3(a)], leading to a robust density of states at the Fermi level. Normalized per formula unit (f.u.) it reads $\mathcal{D}(E_F) = 9.5$ eV^{-1} f.u.$^{-1}$ [Fig. 3(b)]. Most of $\mathcal{D}(E_F)$ originates from electrons in the interstitial space between the muffin-tin spheres, while smaller and more localized contributions from La, Ag, and Pb states make only a negligible contribution to the density of states. The band structure of La_5AgPb_3 follows expectations for quasi-one-dimensional states, as most of the Brillouin zone is populated with virtually dispersionless bands in the ab plane (e.g., Γ-M-K-Γ), while the bands along the chain direction (c axis) Γ-A are strongly dispersing. The flat bands along M-K-Γ are dominated by La states, especially La2 [Fig. 3(a), magenta lines], corroborating their role in the one-dimensional characteristics of La_5AgPb_3. However, not all of the states in La_5AgPb_3 are in the one-dimensional channel, as some dispersing bands on the Brillouin surface can be seen, e.g., along A-L, A-H.

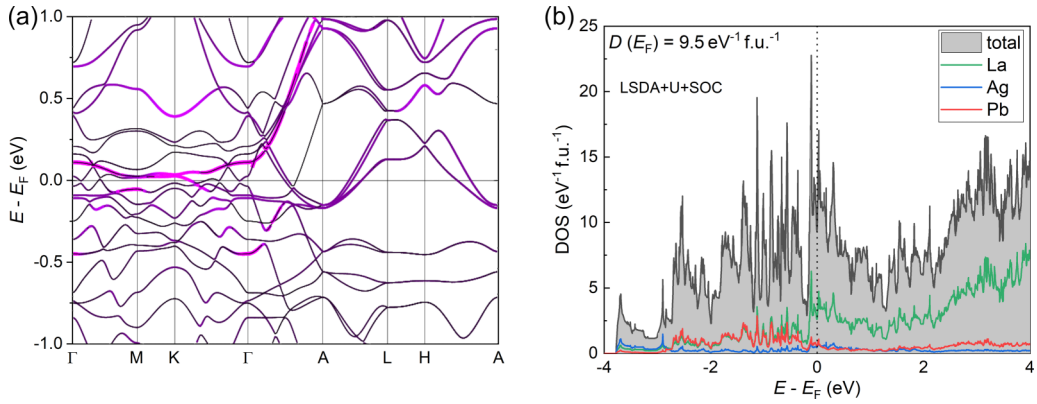

FIG. 3. Density functional calculation results for La_5AgPb_3. (a) Electronic band structure plotted along some high-symmetry directions in the hexagonal unit cell. La2 projections are highlighted in magenta. (b) Electronic density of states as a function of energy E relative to the Fermi energy E_F, with $\mathcal{D}(E_F) = 9.5\ \mathrm{eV}^{-1}\ \mathrm{f.u.}^{-1}$.

We have also calculated the density of valence electrons $n(r)$ of La_5AgPb_3. Representative cuts of $n(r)$ through the (010), (110), and (001) planes are depicted in Fig. 4.

Figure 4(a) shows different planes in the crystal structure of La_5AgPb_3. Starting in Fig. 4(b), we see the projection of $n(r)$ in the (010) plane, which is on the side of the unit cell (blue plane). The most orbital overlap occurs between Ag and La atoms, forming connected paths along the crystallographic c direction, while the Pb atoms in the center are electronically well isolated in this plane. Only minute hybridization between the La1 and Pb orbitals is visible. The quasi-one-dimensional bonding along the c axis between the Ag and La1 atoms is even more apparent from the cut through the center of the unit cell in Fig. 4(d) (green plane). Since the La1 atoms do not lie in the green plane, their electron density is only visible as red blobs close to the Ag atoms on the right- and left-hand sides of the unit cell. The La2 atoms in the center of the plot, however, are electronically isolated, as reflected in the plot in panel (c) (pink plane), where only residual density from the out-of-plane atoms is visible (white bands) between the isolated in-plane La2 and Ag atoms.

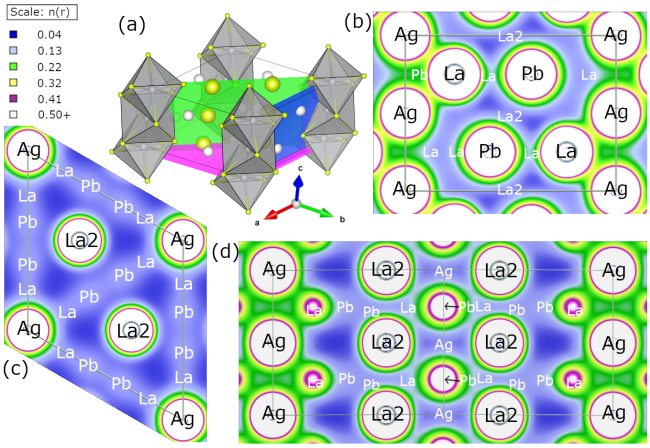

FIG. 4. Density of valence electrons in La_5AgPb_3. Panels (b)–(d) show cuts through the (010), (110), and (001) plane of the hexagonal unit cell (thin gray lines), respectively. (a) The corresponding lattice planes are highlighted in the unit cell in blue, green, and red, respectively. Note that atom labels in white indicate atoms behind and in front of the depicted planes and La1 = La for clarity. The linear color map is truncated at 0.5 electrons per $Å^3$.

It is evident from these plots that the vast majority of the valence electron density is localized around the constituent atoms (see white circles in Fig. 4) with very little density in the interstitial regions. The strongest orbital overlap visible occurs between the irregular La1 octahedra and the enclosed Ag atoms, while the remaining atoms seem electronically well separated from each other, particularly the La2 chains along the c axis.

The results of the valence electron density are suggestive of quasi-one-dimensional behavior in La_5AgPb_3. They imply that substitution of Ag with a magnetic element would likely be the most promising route towards one-dimensional magnetism in this class of materials, since the substitution should be relatively straightforward. Replacing the more isolated La2 atoms would also be interesting, but is much more challenging experimentally, given the presence of the second crystallographic La site in the material. Based on these findings, we hypothesize that magnetic substitution of Ag should lead to more delocalized, itinerant magnetism, while magnetic substitution of the La2 site should lead to well-isolated local moments.

Reports of electride behavior in compounds with similar composition and crystal structure [21,22], and in particular in the Mn_5Si_3 structure type [21], have been published recently. However, we do not see any obvious aggregation of electrons in the interstitial space in La_5AgPb_3, which is the defining characteristic of electride materials. We suggest that this may be because the space in the corners of the unit cell, where such an aggregation is expected to occur (see, e.g., Fig. S2 in Ref. [22]), is occupied by Ag atoms in La_5AgPb_3, unlike the case of Mn_5Si_3 where this site is unoccupied. In any case, our electronic structure calculations do not suggest that La_5AgPb_3 is an electride.

C. Specific heat

The specific heat $C(T)$ of La_5AgPb_3 was measured over the temperature range between 0.05 and 275 K (Fig. 5), where $C(T)$ rises monotonically for temperatures as large

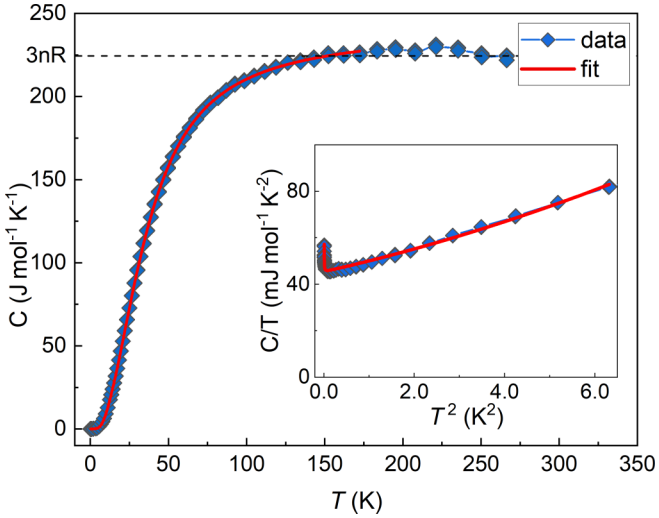

FIG. 5. Specific heat $C(T)$ of La_5AgPb_3 as a function of temperature T between 0.05 and 275 K. The red line is a fit to the data using the Debye-Einstein model defined in the main text. $3nR$ denotes the Dulong-Petit constant with $n = 9$ (dashed line). Inset: Specific heat C/T as a function of T^2 between 0.05 and 2.5 K. The solid red line is a fit to the expression $C(T) = A/T^2 + \gamma T + \beta T^3 + \beta_2 T^5$.

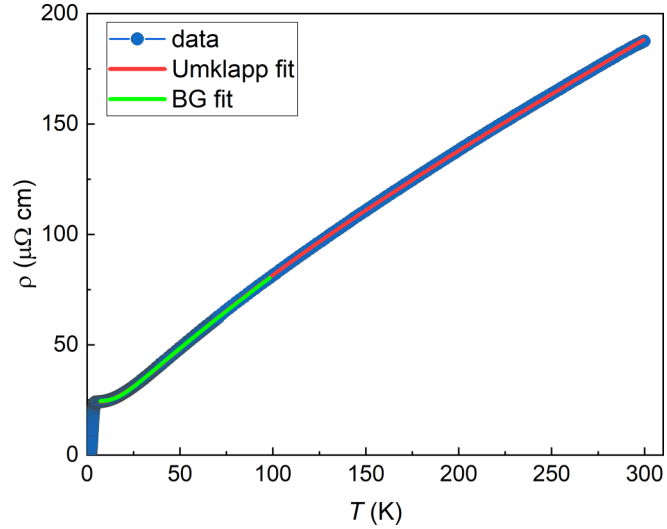

FIG. 6. Temperature dependence of the electrical resistivity $\rho(T)$ of La_5AgPb_3, with the measuring current I applied along the crystallographic c axis. The data (blue symbols) are well described by the modified Bloch-Grüneisen model with an added exponential term to account for phonon-assisted umklapp processes as discussed in the main text (red line). The unaltered Bloch-Grüneisen fit (green line) is also shown.

as $\simeq$250 K. The Debye model gives a poor fit to the overall temperature dependence of $C(T)$, indicating that acoustic phonons alone are not sufficient to describe the specific heat of La_5AgPb_3. We have modeled the measured specific heat C using a Debye-Einstein model that includes both acoustic and optical phonons:

$$C(T) = m_1 C_D(T/T_D) + m_2 C_E(T/T_E). \quad (1)$$

The weighting factors m_i with $i = 1, 2$ enforce the requirement that the acoustic and optical modes must together satisfy the Dulong-Petit limit ($3nR$) at sufficiently large T. Hence, the sum of the weighting factors $\sum m_i$ should approximate the number of atoms per formula unit [23]. We assume in our formula in Eq. (1) that the acoustic modes are described by the Debye term, while the single Einstein mode provides an empirical equivalence of the spectrum of optical modes. The contributions to the specific heat are given by the Debye integral and an Einstein term:

$$C_D = 9R\left(\frac{T}{T_D}\right)^3 \int_0^{T_D/T} \frac{x^4}{(e^x - 1)(1 - e^{-x})} dx,$$

$$C_E = 3R\left(\frac{T_E}{T}\right)^2 \frac{1}{(e^{T_E/T} - 1)(1 - e^{-T_E/T})},$$

with universal gas constant R and Debye and Einstein temperatures T_D and T_E, respectively. The data are well described with the following parameters: $m_1 = 7.9(1)$, $m_2 = 1.5(1)$, $T_D = 159(1)$ K, and $T_E = 52(2)$ K.

A plot of the low-temperature C/T as a function of T^2 (Fig. 5, inset) reveals a sharp increase below 0.75 K indicative of a nuclear Schottky anomaly, likely associated with the large nuclear spin $I = 7/2$ of ^{139}La. We therefore fit the low-temperature C/T for temperatures between 0.07 and 2.5 K to the expression $C(T) = A/T^2 + \gamma T + \beta T^3 + \beta_2 T^5$. The first term describes the high-temperature tail of the Schottky anomaly with $A = R_0\Delta/4$, where $R_0 = 8.314$ J mol^{-1} K^{-1} and energy gap Δ. The fit is well described with the following parameters: $A = 4.0(1)$ nJ K mol^{-1}, $\gamma = 45.4(1)$ mJ mol^{-1} K^{-2}, $\beta = 4.4(2)$ mJ mol^{-1} K^{-4}, and $\beta_2 = 0.24(3)$ mJ mol^{-1} K^{-6}. The A parameter corresponds to an energy gap Δ associated with the Schottky anomaly of $\Delta = 1.4(1)$ mK. The Debye temperature is calculated using $\beta = (12\pi^4/5)nN_A k_B/T_D^3$, which leads to $T_D = 158.3(3)$ K, in excellent agreement with the value found above. The Sommerfeld coefficient corresponds to $\mathcal{D}(E_F) = 19.3(1)$ eV^{-1} f.u.$^{-1}$ at the Fermi level. Given our calculated density of states determined $\mathcal{D}(E_F) = 9.5$ eV^{-1} f.u.$^{-1}$, this leads to a mass enhancement factor $(1 + \lambda) = 2.03$, where $(1 + \lambda) = 3\gamma[k_B\pi\mathcal{D}(E_F)]^{-1}$. This comparison indicates that electronic correlations are moderate in La_5AgPb_3, leading to a small mass enhancement that is in line with observations in similar materials with the same crystal structure, such as La_5Ge_3 (33.6 mJ mol^{-1} K^{-2}) and La_5Si_3 (27.0 mJ mol^{-1} K^{-2}) [24], but not La_5Pb_3 (6.5 mJ mol^{-1} K^{-2}) [25].

D. Electrical resistivity

The electrical resistivity $\rho(T)$ of La_5AgPb_3 (Fig. 6) is of order 100 $\mu\Omega$ cm at room temperature, indicating metallic behavior in agreement with our DFT results. Accordingly, $\rho(T)$ decreases monotonically with decreasing temperature, initially being sublinear but becomes linear between 100 and 35 K before it flattens out with a residual value of 24 $\mu\Omega$ cm at 5 K. This results in a residual resistivity ratio of $\rho(295\text{ K})/\rho(5\text{ K}) = 8$, indicating sizable scattering at low temperatures. Below 4.2 K the resistivity drops sharply, indicating a transition into a superconducting state. However, the broad superconducting transition is not complete, as the

resistivity remains nonzero down to the lowest measured temperature of 1.8 K. No evidence for a superconducting transition was found in the specific heat or magnetization measurements of our crystals. We believe that a thin layer of $LaPb_3$ with a superconducting transition temperature $T_c = 4.18$ K [26] is responsible. Since $LaPb_3$ is a decomposition product of La_5AgPb_3, we speculate that it formed on the surface as the sample was briefly exposed to air as it was transferred into the measurement device. No indications for the presence of $LaPb_3$ have been observed in either our EDX or our XRD analysis.

The resistivity in the temperature range 5–100 K is well described by the Bloch-Grüneisen law:

$$\rho(T) = \rho_0 + \rho_D(T), \tag{2}$$

$$\rho_D(T) = A\left(\frac{T}{T_D}\right)^5 \int_0^{T_D/T} \frac{x^5 dx}{(e^x - 1)(1 - e^{-x})}, \tag{3}$$

where $A = 254.6(6)$ $\mu\Omega$ cm, $T_D = 105.2(2)$ K, and $\rho_0 = 24.49(2)$ $\mu\Omega$ cm. This indicates that the scattering of weakly correlated quasiparticles from acoustic phonons is dominant in this temperature range.

The Debye temperature obtained from this analysis is significantly smaller than the 159 K found in the specific heat measurement, although its value does depend to some extent on the temperature range for the Bloch-Gruneisen fit. However, enforcing $T_D = 159$ K in the above fit does not describe the data well. Adding a term $\rho_{el}(T) = AT^2$ to account for electron-electron scattering within Fermi liquid theory did not improve the fit, and in fact the A parameter was refined to zero.

In an attempt to describe $\rho(T)$ over the full measured temperature range, we added an Einstein term, $\rho_E(T) = (B/T)/[(e^{T_E/T} - 1)(1 - e^{-T_E/T})]$, to the model [27], as in the analysis of the specific heat. This did not improve the quality of the fit. However, adding an exponential term, $B\exp(-T_0/T)$, that accounts for umklapp processes assisted by a specific phonon with an energy T_0 [28,29], gives an excellent fit to the data (Fig. 6, red line) over the entire measured temperature range when we enforce $T_D = 159$ K, which yields the following parameters: $A = 317.0(4)$ $\mu\Omega$ cm, $B = 20.5(2)$ $\mu\Omega$ cm, $T_0 = 38.6(4)$ K and $\rho_0 = 24.14(4)$ $\mu\Omega$ cm. T_0 is comparable in size to T_E found above. We have recently observed similar behavior in superconducting La_2Ni_2In [30].

E. Magnetic susceptibility

The dc magnetic susceptibility $\chi(T)$ of La_5AgPb_3 with the magnetic field H applied along the crystallographic c direction is only weakly temperature dependent over the measured temperature range 1.8–400 K [Fig. 7(a)]. $\chi(T)$ increases slightly with decreasing temperature until ~60 K where a broad maximum forms. A rapid increase in $\chi(T)$ indicative of a Curie-Weiss tail, presumably from paramagnetic impurities, is observed below 15 K. Assuming $S = 1/2$ for the impurities, the associated Curie constant of $C_{para} \approx 2 \times 10^{-4}$ cm^3 mol^{-1} K corresponds to an impurity concentration of $n_{para} = 4.3 \times 10^{-4}$ mol^{-1}, i.e., 0.04 %.

$\chi(T)$ exhibits a weak field dependence, particularly in smaller magnetic fields [Fig. 7(a)]. This indicates the presence of a spontaneous magnetization M_0, likely introduced

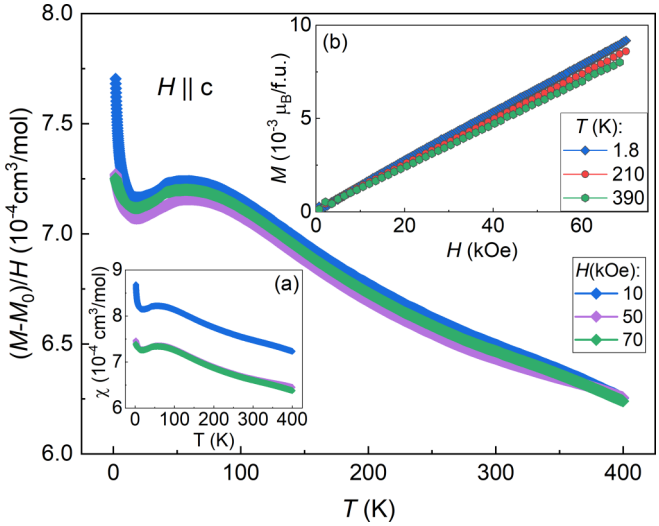

FIG. 7. (a) The temperature dependencies of the magnetic susceptibility $\chi(T)$, measured in fields of 10 kOe (blue), 50 kOe (violet), and 70 kOe (green) that were applied parallel to the crystallographic c axis. Main panel: Subtracting a constant magnetization $M_0 = 0.98$ emu/mol removes the field dependence of the dc magnetization. (b) The field dependencies of the magnetization M measured at different temperatures.

by a tiny amount of ferromagnetic impurities in the sample. Subtracting a small constant $M_0 = 0.98$ emu/mol $\approx 1.76 \times 10^{-4}$ μ_B/f u. from the data makes the measurements taken at different fields virtually collapse on top of each other (Fig. 7, main panel), corroborating this hypothesis. Taking $M_0 \sim 1$ μ_B/atom we can estimate this ferromagnetic impurity concentration $n_{FM} = 0.002$ % present in the sample. This is far below the sensitivity limits of most analytical methods, including XRD and EDX.

However, the spontaneous moment M_0 does not explain the Curie tail visible in Fig. 7 at the lowest temperatures. This tail is more pronounced in low magnetic fields, indicating that these paramagnetic impurities can be saturated in moderate applied fields. To reduce the contributions from both paramagnetic and ferromagnetic impurities we extract the susceptibility χ_0 instead from the isotherms of the magnetization $M(H)$.

$M(H)$ exhibits a linear dependence on magnetic field above 10 kOe at all measured temperatures [Fig. 7(b)]. By extracting the slope of the $M(H)$ curves from a linear fit to the data between 10 and 70 kOe [average $\chi_{red.} = 0.009(8)$, $R^2 = 0.999\,93(7)$] we effectively remove all contributions by impurities that are fully magnetized in that field range, as they do not contribute to the slope of $M(H)$ anymore. The resulting susceptibility $\chi_0 = dM/dH$ is virtually identical to the corrected data depicted in Fig. 7 (main panel), but without the pronounced impurity tail at low temperatures (Fig. 8). As well, the observed weak maximum is shifted to slightly higher temperatures (~75 K). We note that this procedure does not remove contributions from impurities that are not fully magnetized in the selected fit range, which will be further discussed below.

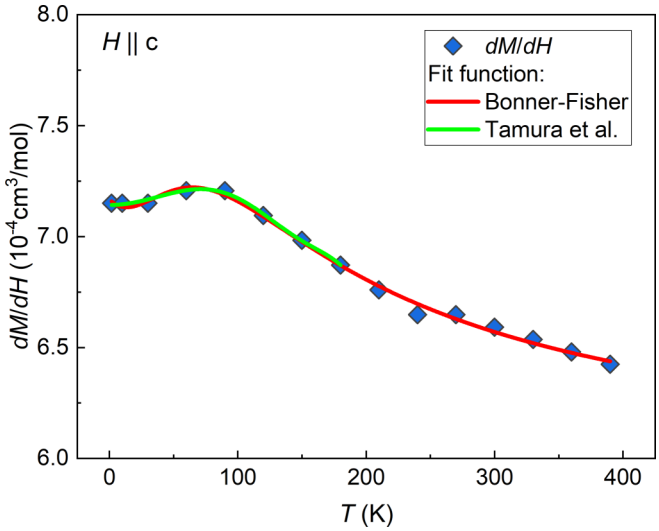

FIG. 8. Effective susceptibility $\chi_0 = dM/dH$ of La_5AgPb_3 as a function of temperature T, determined from $M(H)$ data as described in the main text. The magnetic field was applied parallel to the crystallographic c axis. Solid lines depict fits to the Bonner-Fisher model and the phenomenological expression from Ref. [31].

Intriguingly, similar maxima in the magnetic susceptibility have been observed in quasi-one-dimensional conductors such as TTF-TCNQ (tetrathiafulvalene-tetracyanoquinodimethane) [32,33], and related systems [31,34]. The maxima are taken as evidence for electronic correlations, that as well result in an overall enhancement of the magnetic susceptibility beyond the value in a corresponding system with noninteracting electrons [32]. Tight-binding calculations and the Hubbard model adequately reproduce the high-temperature part of the magnetic susceptibility in these quasi-one-dimensional metals. In the limit of strong Coulomb interaction the magnetic part of the Hubbard model can in fact be equated to a Heisenberg linear chain of spins and it is found that the Bonner-Fisher (BF) model [35] provides an adequate description of the measured susceptibility. Similar maxima have also been observed in other materials such as Tb_2PdSi_3 and $LaNiO_3$ [36,37].

We have, therefore, compared our corrected susceptibility χ_0, to the following expression: $\chi_0 = \chi_{BF} + \chi_{CW} + \chi_P$, with χ_{BF} the polynomial expansion of the Bonner-Fisher model [38], $\chi_{CW} = C/(T - \theta)$ a Curie-Weiss term with Curie constant C and temperature θ, and χ_P the temperature-independent Pauli susceptibility (see red line in Fig. 8). Note, that we included a Curie-Weiss term to account for any remaining paramagnetic impurities that are not saturated in fields as large as 7 T. The BF fit describes the data very well and leads to an effective moment of $\mu_{eff} = 0.50(1)\,\mu_B$ per formula unit, an exchange constant of $J/k_B = 61(4)$ K, and a Pauli susceptibility of $\chi_P = 5.9(6) \times 10^{-4}$ cm^3 mol^{-1}. The latter corresponds to a DOS $\mathcal{D}(E_F) = 18.25(4)$ eV^{-1} f.u.$^{-1}$, which is in very good agreement with the value determined from our specific heat data [19.26(5) eV^{-1} f.u.$^{-1}$]. Accordingly, the Wilson ratio $R_W = \chi_P/\gamma = 0.95$ indicates that there is no ferromagnetic enhancement of the density of states in La_5AgPb_3. The overall magnitude of χ_0 is enhanced by a factor of ~2 compared to the expected Pauli susceptibility $\chi_P = 3.1 \times 10^{-4}$ cm^3 mol^{-1}, given our calculated density of states $\mathcal{D}(E_F) = 9.5$ eV^1 f.u.$^{-1}$.

However, since we have no independent evidence that the Coulomb interaction has led to localized and moment-bearing electron states in La_5AgPb_3, we present as well a more phenomenological description [31], where electronic correlations lead to spin fluctuations with a characteristic temperature scale T^* that corresponds to the temperature where χ has a maximum, i.e., 75 K in La_5AgPb_3. The fit to this model (Fig. 8, green line) describes the data at low temperatures as well as the Bonner-Fisher expression. The observation of Fermi liquid behaviors at low temperature in the low-temperature specific heat, as well as the modest enhancements of the Sommerfeld coefficient, and the Pauli susceptibility all lend credence to this second interpretation. It is worth noting that the inferred spin fluctuations in La_5AgPb_3 have a significantly smaller scale $T^* = 75$ K than those found in the quasi-one-dimensional metals, where higher values of T^* indicate significantly stronger electronic correlations.

Overall, our analysis of the temperature dependence of the magnetic susceptibility lends further evidence that there are electronic states in La_5AgPb_3 with one-dimensional character. We caution that not all of the states at the Fermi level are necessarily one-dimensional, but may instead contribute to the temperature-independent Pauli susceptibility.

IV. CONCLUSION

We now discuss where La_5AgPb_3 fits among the different quasi-one-dimensional systems that have been experimentally identified so far. There is sustained interest in quasi-one-dimensional systems, due to the exotic nature of their excitations. Experiments carried out on insulating spin chains have given much insight into these excitations, and provide a direct connection to exact theoretical results and numerical computations [4,5]. More recently these sorts of experiments have been extended to quasi-one-dimensional systems that are conducting, where the f-electron based spin chains are weakly coupled to a conduction electron system [39,40]. In both these insulating and metallic systems, the moment-bearing electrons are localized, and so they are excluded from the states contained by the Fermi level. This is clearly not the case for La_5AgPb_3 where there are no localized magnetic moments. The earliest studied examples of quasi-one-dimensional conductors had no d- or f-electron based magnetism, only conduction electron spin itself. Consistent with theoretical expectations, fractionalized excitations were observed in these systems [6,7]. Electronic correlations were found to be minimal in these latter systems, and so the Fermi surface contains all the electron states contributed by the constituent atoms. The conducting one-dimensional systems contain physics that is absent in the insulating spin-chain systems. Namely, an electron delocalization transition akin to a Mott transition is expected, with the localized f-electron spin-chain systems being on the correlated side of that transition and the conduction electron based systems on the delocalized side. In this way, we assign La_5AgPb_3 to the latter category.

Conducting systems where that delocalization transition can be studied constitute a pressing need to complete this analogy between electron delocalization transitions in one and three dimensions [8]. We presented here experimental and theoretical evidence that La_5AgPb_3 is quasi-one-dimensional, and the absence of d- or f-electron based magnetic character and its moderate correlations indicate that it is on the delocalized side of that transition with all states contained by the Fermi surface. Future work will focus on identifying new members of this family of compounds that are closer to the putative electronic delocalization transition where correlations could be strengthened, along with the outright magnetic character and also order that are expected on the localized side of that transition.

We have synthesized high-quality single crystals of La_5AgPb_3 from flux and reported their physical properties, including magnetization, specific heat, and electrical resistivity. Given the quasi-one-dimensional character of the underlying crystal lattice, our objective was to assess La_5AgPb_3's suitability as a benchmark system as indicated above. The benchmark is a quasi-one-dimensional system without local moments and without substantial correlations that would generate localized magnetic moments or render it insulating. Considering the moderate correlations, lack of localized moments, and DFT computations revealing the presence of hybridized Ag atoms as well as electronically well isolated La2 atoms that extend along the c axis, La_5AgPb_3 appears to be suitable. Given the compositional flexibility of this structure type [9,11], these results are very encouraging that correlations and magnetism could be added, either by substituting moment-bearing transition metal atoms for Ag, or rare earths for the La2 atoms.

The electronic structure calculations confirm expectations that La_5AgPb_3 has a robust and apparently conventional Fermi surface, and this result is verified by measurements of the specific heat, indicating that La_5AgPb_3 displays Fermi liquid behavior at the lowest temperatures. While this would not be expected for a truly one-dimensional system, it is rare that transport or thermal measurements find evidence for the Luttinger liquid behavior that is expected [41]. The complexity of the Fermi surface, which is comprised of five different bands, raises a legitimate concern that not all of those bands are necessarily quasi-one-dimensional. Spectroscopic investigations are required to definitively determine whether spinons and holons, the signature excitations of one-dimensional systems, are present in La_5AgPb_3.

Comparing the Sommerfeld coefficient of the specific heat to the values determined by the DFT computations indicates that the electronic correlations are moderate. In agreement, the temperature-independent part of the magnetic susceptibility shows no enhancement relative to the density of states construed from the Sommerfeld constant, giving the Wilson constant $R_W = 0.95$. This indicates that La_5AgPb_3 does not have significant ferromagnetic fluctuations. These results suggest that La_5AgPb_3 is a moderately correlated metal, with a crystal structure that is suggestive of quasi-one-dimensional character. The spectrum of one-dimensional systems that are currently known starts with the insulating spin chains, where the correlations are so strong that they localize electrons and form robust magnetic moments. Neutron scattering experiments find fractionalized excitations, proof of the electronic one-dimensionality of these systems. Fractionalized excitations are similarly observed in Yb_2Pt_2Pb [39,40], where the localized moments of the f electrons of the Yb atoms form chains that are only weakly hybridized with the conduction electrons of this excellent metal. Decreasing the correlations leads to the delocalization of electrons and the collapse of magnetic moments at a Mott transition or crossover. The molecular conductors like TTF-TCNQ are apparently on the delocalized side of a Mott transition, where the extended states are still highly correlated. Provided that spectroscopic measurements find that La_5AgPb_3 is truly one-dimensional, it would be by far the most weakly correlated system yet identified. The flexibility of the R_5MX_3 (R = rare earth, M = transition metal or main group element, X = Pb, Sn, Sb, In, Bi) family of compounds is quite promising that new compounds with moderate degrees of correlations and magnetism can be explored.

ACKNOWLEDGMENTS

We acknowledge support by the Natural Sciences and Engineering Research Council of Canada (NSERC). This research was supported by Grant No. NSF-DMR-1807451. J.M. was supported in part by funding from the Max Planck-UBC-UTokyo Centre for Quantum Materials and the Canada First Research Excellence Fund, Quantum Materials and Future Technologies Program. We thank Ilya Elfimov for useful discussions.

[1] F. Steglich and S. Süllow, in *Encyclopedia of Materials: Science and Technology*, edited by K. J. Buschow, R. W. Cahn, M. C. Flemings, B. Ilschner, E. J. Kramer, S. Mahajan, and P. Veyssire (Elsevier, Oxford, 2001), pp. 3746–3749.
[2] D. C. Johnston, Adv. Phys. **59**, 803 (2010).
[3] P. Coleman and A. J. Schofield, Nature (London) **433**, 226 (2005).
[4] B. Lake, A. M. Tsvelik, S. Notbohm, D. A. Tennant, T. G. Perring, M. Reehuis, C. Sekar, G. Krabbes, and B. Büchner, Nat. Phys. **6**, 50 (2010).
[5] M. Mourigal, M. Enderle, A. Klöpperpieper, J.-S. Caux, A. Stunault, and H. M. Rønnow, Nat. Phys. **9**, 435 (2013).
[6] R. Claessen, M. Sing, U. Schwingenschlögl, P. Blaha, M. Dressel, and C. S. Jacobsen, Phys. Rev. Lett. **88**, 096402 (2002).
[7] L. Dudy, J. Denlinger, J. Allen, F. Wang, J. He, D. Hitchcock, A. Sekiyama, and S. Suga, J. Phys.: Condens. Matter **25**, 014007 (2012).
[8] K. Kanoda and R. Kato, Annu. Rev. Condens. Matter Phys. **2**, 167 (2011).
[9] A. M. Guloy and J. D. Corbett, J. Solid State Chem. **109**, 352 (1994).
[10] W. Rieger and E. Parthé, Monatsh. Chem./Chemical Monthly **99**, 291 (1968).
[11] L. Gulay, J. Alloys Compd. **392**, 165 (2005).

[12] P. C. Canfield, T. Kong, U. S. Kaluarachchi, and N. H. Jo, Philos. Mag. **96**, 84 (2016).
[13] P. Blaha, K. Schwarz, F. Tran, R. Laskowski, G. K. Madsen, and L. D. Marks, J. Chem. Phys. **152**, 074101 (2020).
[14] J. P. Perdew, K. Burke, and M. Ernzerhof, Phys. Rev. Lett. **77**, 3865 (1996).
[15] V. Tran, M. Gamża, A. Ślebarski, J. Jarmulska, and W. Miiller, J. Solid State Chem. **180**, 2756 (2007).
[16] V. Goruganti, K. Rathnayaka, J. H. Ross, Jr., and Y. Öner, J. Appl. Phys. **103**, 07B709 (2008).
[17] V. Goruganti, K. Rathnayaka, and J. H. Ross, Jr., J. Appl. Phys. **105**, 07E118 (2009).
[18] P. C. Canfield, Rep. Prog. Phys. **83**, 016501 (2019).
[19] A. V. Fedorov, C. Laubschat, K. Starke, E. Weschke, K.-U. Barholz, and G. Kaindl, Phys. Rev. Lett. **70**, 1719 (1993).
[20] J. Lang, Y. Baer, and P. Cox, J. Phys. F: Met. Phys. **11**, 121 (1981).
[21] C. Liu, S. A. Nikolaev, W. Ren, and L. A. Burton, J. Mater. Chem. C **8**, 10551 (2020).
[22] Q. Zhu, T. Frolov, and K. Choudhary, Matter **1**, 1293 (2019).
[23] B. F. Woodfield, J. Boerio-Goates, J. L. Shapiro, R. L. Putnam, and A. Navrotsky, J. Chem. Thermodyn. **31**, 245 (1999).
[24] N. Gorbachuk, A. Bolgar, A. Blinder, and O. Boetskaya, Powder Metall. Met. Ceram. **37**, 298 (1998).
[25] J. T. Demel, Low temperature heat capacity of YPb_3, $LaPb_3$, La_5Pb_3 and La_5Pb_3C, Ph.D. thesis, Iowa State University, 1973, https://core.ac.uk/download/pdf/38913543.pdf.
[26] L. Welsh, C. Wiley, and F. Fradin, Phys. Rev. B **11**, 4156 (1975).
[27] J. Cooper, Phys. Rev. B **9**, 2778 (1974).
[28] D. W. Woodard and G. D. Cody, Phys. Rev. **136**, A166 (1964).
[29] M. Milewits, S. J. Williamson, and H. Taub, Phys. Rev. B **13**, 5199 (1976).
[30] J. Maiwald, I. I. Mazin, A. Gurevich, and M. Aronson, Phys. Rev. B **102**, 165125 (2020).
[31] M. Tamura, Y. Kashimura, H. Sawa, S. Aonuma, R. Kato, and M. Kinoshita, Solid State Commun. **93**, 585 (1995).
[32] J. Torrance, Y. Tomkiewicz, and B. Silverman, Phys. Rev. B **15**, 4738 (1977).
[33] J. C. Scott, S. Etemad, and E. M. Engler, Phys. Rev. B **17**, 2269 (1978).
[34] S. Klotz, J. S. Schilling, M. Weger, and K. Bechgaard, Phys. Rev. B **38**, 5878 (1988).
[35] J. C. Bonner and M. E. Fisher, Phys. Rev. **135**, A640 (1964).
[36] P. L. Paulose, E. V. Sampathkumaran, H. Bitterlich, G. Behr, and W. Löser, Phys. Rev. B **67**, 212401 (2003).
[37] J. Zhang, H. Zheng, Y. Ren, and J. Mitchell, Cryst. Growth Des. **17**, 2730 (2017).
[38] W. E. Hatfield, J. Appl. Phys. **52**, 1985 (1981).
[39] L. Wu, W. Gannon, I. Zaliznyak, A. Tsvelik, M. Brockmann, J.-S. Caux, M. Kim, Y. Qiu, J. Copley, G. Ehlers *et al.*, Science **352**, 1206 (2016).
[40] W. Gannon, I. A. Zaliznyak, L. Wu, A. Feiguin, A. Tsvelik, F. Demmel, Y. Qiu, J. Copley, M. Kim, and M. Aronson, Nat. Commun. **10**, 1123 (2019).
[41] T. Giamarchi, in *Topological Phase Transitions and New Developments* (World Scientific, Singapore, 2019), pp. 147–164.